Synthesis and Physical Characterization of Novel Heme-Based Model Systems for Photoinitiated Electron Transfer. 1. Complexation of a RuProHis Bifunctional Peptide and Microperoxidase-11†

B. Fan,‡ D. L. Fontenot,§ R. W. Larsen,|| M. C. Simpson,⊥ J. A. Shelnutt,⊥ R. Falcon,‡ L. Martinez,‡ S. Niu,|| S. Zhang,‡ T. Niemczyk,‡ and M. R. Ondrias*,‡

Department of Chemistry, University of New Mexico, Albuquerque, New Mexico 87131, Life Sciences Division, Los Alamos National Laboratory, Los Alamos, New Mexico 87545, Department of Chemistry, University of Hawaii, Honolulu, Hawaii 96822, and Fuel Sciences Division, Sandia National Laboratory, Albuquerque, New Mexico 87185

Received January 15, 1997⊗

This paper describes the synthesis and initial physical characterization of a new type of model system for the investigation of photoinitiated electron transfer (ET) in proteins and polypeptides. This system is based upon a derivative of a heme-containing digestion product of cytochrome *c*, microperoxidase-11 (MP-11). The vacant axial position of the five-coordinate heme of MP-11 is coordinated to the terminal histidine of a dipeptide having a photoactive ruthenium tris(bipyridine) moiety at its other end (RuProHis). Photoexcitation of the ruthenium group results in rapid ($k_{ET} > 10^7\ s^{-1}$), reversible ET to the ferric heme. The equilibrium properties of MP-11 and the MP-11/Ru(peptide) complex were characterized with optical absorption, luminescence, and resonance Raman (RR) spectroscopies. Molecular modeling was also employed to examine the structure and energetics of the equilibrium species. Clear evidence for reversible photoinduced ET was observed in time-resolved luminescence and transient resonance Raman studies of the MP-11/RuProHis samples.

Introduction

Physical studies of biological systems aim at revealing the exact molecular bases for their function. Because of the complexity of most biological systems, it is usually more practical to examine the behavior of simpler yet relevant model systems. In addition to contributing to the understanding of basic mechanisms of biological function, the study of model systems has potential importance in the manufacture of artificial biomimetic devices. One such area in which model system design has found wide application is the study of biological electron transfer.[1] Most current model systems are based on the use of a conventional chemical species to mimic only the active sites of native proteins. To date, few efforts have been made to use protein fragments as integral parts of model systems.[2] Here we describe the synthesis of a new class of model electron transfer systems based upon the coordination of a photoactive ruthenated peptide to heme-containing fragments of cytochrome *c*. Initial spectroscopic and photophysical studies of these model systems show that, while bearing most of the desirable features of inorganic model systems (solubility, stability, etc.), they offer some unique opportunities for probing some of the less well-understood aspects of biological electron transfer (ET) processes.

Microperoxidases are products of proteolytic digestion of cytochrome *c*. Using different combinations of pepsin and trypsin, three different species containing the heme active site and eight, nine, or eleven amino acids can be prepared.[3] In all three digestion fragments, the short peptides remain covalently linked to the heme with the two thioether bonds between cys-14 and cys-17, and histidine-18 is still coordinated to the heme through its imidazole nitrogen. This unique structure preserves many of the basic heme−protein bonding interactions present in cytochrome *c* while offering a much simpler system that can be systematically modified by covalent or coordinative binding of photoactive species.

Derivatives of ruthenium polypyridyl complexes are widely used to photoinitiate ET reactions in biological systems because of their useful photoelectrochemical properties.[4] Chemical derivatization of the bipyridine ligand allows the attachment of different reactive groups to the complex. These, in turn, can be used to covalently modify specific amino acid residues of native proteins[5] or functionalized peptides. ET processes can be initiated in these types of systems in a well-defined manner

* To whom correspondence should be addressed.

† Abbreviations used: ET, electron transfer; MLCT, metal to ligand charge transfer; CLS, classical least-squares progression; RR, resonance Raman; MP-11, microperoxidase-11 (heme undecapeptide); acMP-11, microperoxidase-11 acetylated at both amino groups as described in the text; RuProHis, $(bpy)_2Ru$(4-methyl-4′-(histidylprolyl)bpy), where bpy = 2,2′-bipyridine (see text for details).

‡ University of New Mexico.

§ Los Alamos National Laboratory.

|| University of Hawaii.

⊥ Sandia National Laboratory.

⊗ Abstract published in *Advance ACS Abstracts*, August 1, 1997.

(1) (a) Gust, D.; Moore, T. A.; Moore, A. L. *Acc. Chem. Res.* **1993**, *26*, 198. (b) Wasielewski, M. R. *Chem. Rev.* **1992**, *92*, 435. (c) Orman, L. K.; Anderson, D. R.; Yabe, T.; Hopkins, J. B. In *Electron Transfer in Biology and the Solid State*; Johnson, M. K., et al., Eds.; American Chemical Society: Washington, DC, 1990. (d) Fox, M. A., Chanon, M., Eds. *Photoinduced Electron Transfer*; Elsevier: New York, 1988; Parts A−D.

(2) Low, D. W.; Winkler, J. R.; Gray, H. B. *J. Am. Chem. Soc.* **1996**, *118*, 117.

(3) (a) Kraehenbuhl, J. P.; et al. *J. Exp. Med.* **1974**, *139*, 208. (b) Harbury, H. A.; Loach, P. A. *J. Biol. Chem.* **1960**, *235*, 3640.

(4) (a) Kalyanasundaram, K. *Coord. Chem. Rev.* **1982**, 46, 159. (b) Juris, A.; Balzani, V.; Barrigelletti, F.; Campagna, S.; Belser, P.; Von Zelewsky, A. *Coord. Chem. Rev.* **1988**, *84*, 85.

(5) (a) Bjerrum, J. M.; Casimiro, D. R.; Wuttke, D. S. *J. Bioenerg. Biomembr.* **1995**, *27*, 295. (b) Geren, L. M.; Beasley, J. R.; Millett, F. *J. Biol. Chem.* **1995**, *270*, 2466. (c) Winkler, J. R.; Gray, H. B. *Chem. Rev.* **1992**, *92*, 375. (d) Gray, H. B.; Winkler, J. R. *Pure Appl. Chem.* **1992**, *64*, 1257. (e) Winkler, J. R.; Malmstrom, B. G.; Gray, H. B. *Biophys. Chem.* **1995**, *54*, 199. (f) Wuttke, D. S.; Winkler, J. R.; Gray, H. B. *Science* **1992**, *256*, 1007.

(6) Isied, S. S.; Ogawa, M. Y.; Wishart, J. F. *Chem. Rev.* **1992**, *92*, 381.

S0020-1669(97)00041-4 CCC: $14.00

by photoexcitation of the ruthenium MLCT band to produce a long-lived, redox-active excited state. This general strategy has been particularly useful for spectroscopic investigations of the ET kinetics of heme proteins.[5]

The most attractive feature of ruthenium/heme systems is their spectroscopic versatility. Both the donor ($Ru(bpy)_3^{2+}$*) and acceptor (heme) groups can be probed by a variety of different spectroscopic methods. Absorption spectroscopy can be applied to the characterization of the ground and excited states of both chromophores. In addition, the quenching of intrinsic $Ru(bpy)_3^{2+}$* luminescence can be monitored to determine the kinetics of competing deactivation pathways. Another spectroscopic advantage of these systems is that both the ruthenium polypyridyl donors and heme acceptors are excellent resonance Raman scatterers.[7] Moreover, their individual vibrational spectra can be easily isolated by appropriate tuning of the excitation wavelength. In particular, the huge difference in resonance Raman cross sections at the heme absorption maximum (~400 nm) allows the selective investigation of the heme without interference from the donor. Luminescence generally presents a major obstacle for Raman experiments of photoactive chromophores since most emission processes occur with much greater intensity than the Raman scattering itself. Fortunately, hemes are nonfluorescent and the emission of $Ru(bpy)_3^{2+}$ occurs at wavelengths that do not overlap with the Raman signal from the heme. This makes it possible to use Raman scattering to selectively study the transient behavior of the heme during and subsequent to photoinduced ET.

This work describes our recent efforts to design and synthesize a versatile set of model systems which combine the essential features of the cytochrome *c* active site with ruthenium tris(bipyridine) based photoinitiation of the ET process. It was demonstrated previously that histidine-containing peptides readily form coordination complexes with microperoxidases.[8b] We have expanded upon these results to create a family of short bifunctional peptides with histidine and ruthenium-derivatized ends separated by proline spacers. These can be coordinated to MP-11, forming a series of electron transfer model complexes in which ET can be photoinitiated and then followed spectroscopically. The relative simplicity of these $Ru(Pro)_nHis$ systems offers a unique opportunity to address specific structural aspects of the electron transfer process. This report concentrates on the synthesis and characterization of the prototypic member of this series, the RuProHis/MP-11 complex.

Materials and Methods

Spectroscopies. For all spectroscopic experiments, the concentrations of MP-11 and RuProHis were determined using extinction coefficients of $\epsilon_{396} = 150\,000\ M^{-1}\ cm^{-1}$ and $\epsilon_{290} = 87\,000\ M^{-1}\ cm^{-1}$ for MP-11[8a] and RuProHis,[4] respectively. The relative extinction coefficients of acMP-11 and MP-11 at 670 nm were estimated from spectra normalized at the Soret band. Because RuProHis slowly hydrolyzes in aqueous solution, especially at acidic pH values, samples were always stored as powders and dissolved in appropriate buffer immediately prior to the experiments. All samples were deoxygenated by Ar purging for 20 min immediately before the experiments. UV−vis absorption measurements were obtained with a Hewlett-Packard HP8452A diode array spectrophotometer. Static luminescence spectra were obtained with a Perkin-Elmer PL-5 fluorometer.

The transient luminescence experiments were performed using intrumentation described by Larsen and co-workers.[9] Briefly, the sample was excited with a 532 nm laser pulse (7 ns, 150 mW, 10 HZ) from the second harmonic of a Q-Switched Nd:YAG laser (Surelite II, Continuum). The emission was collected and imaged onto the entrance slit of a Spex 1680B double monochromator. The signal was detected using a Hamamatsu R928 photomultiplier tube and amplified using a 500 MHz preamplifier. The signal was digitized and recorded with an IBM 486 based computer. Resonance Raman (RR) spectra were obtained via protocols described in the following article.

Synthesis and Characterization of Ruthenated Peptides. The synthesis of the reactive precursor, the *N*-hydroxysuccinyl ester of [bis(2,2′-bipyridine)(4′-methyl-2,2′-bipyridine-4-carboxylic acid)Ru^{II}]$(PF_6)_2$, RumOH, was performed by using the procedure of Peek et al with minor modifications.[10] The synthesis of RuProHis was performed using manual methods on a Rapid Multiple Peptide Synthesizer (RaMPS) (DuPont, Boston, MA) and 0.1 mM Rapid Amide (2,3-bis(methyloxy)-benzhydrylamine) resin cartridges (DuPont, Boston, MA). The deprotection reagents were anhydrous piperidine and trifluoroacetic acid (Sigma, St. Louis, MO). The scavengers 1,2-ethanedithiol, thioanisole, and anisole were purchased from DuPont (Boston, MA). The Fmoc amino acids, histidine, and proline were purchased from Advanced Chem Tech (Louisville, KY). Histidine side chains were protected with the triphenylmethyl group.

The amino acids and Ru-mOH were coupled as active esters of 1-hydroxybenzotriazole (HOBt). The coupling reactions using 0.1 mmol of HOBt-activated amino acids were performed in 2 mL of DMF and 1 mL of DCM for 1 h at room temperature. Ninhydrin reactions were performed at the completion of each coupling reaction using a ninhydrin test kit purchased from DuPont (Boston, MA).

The Fmoc protecting group was removed at the completion of a synthetic cycle by shaking the solution for 20 min in 3 mL of a 50:50 piperidine:DMF mixture, followed by extensive washing with DMF and methanol. The removal of side chain protecting groups and cleavage of the peptides from the resins were performed by shaking in 3 mL of a 90:5:3:2 TFA:thioanisole:1,2-ethanedithiol:anisole solution for 4 h at room temperature in 5 mL a polypropylene Quick-Sep disposable chromatography columns from Isolab (Akron, OH). The TFA and peptide mixture was drained from the column into cold water, extracted three times with water, and lyophilized.

The crude peptides were purified by reverse-phase HPLC using a Waters 600E chromatograph with a Waters 486 absorption detector. Analytical separation utilized a Delta Pak C18 300 A (3.9 × 300 mm) RP-HPLC column, and semipreparative separations used a Waters C18 (7.8 × 300 mm) column. Chromatography solvents were HPLC grade acetonitrile and water, both containing 0.1% TFA. The purification was performed using a 1%/min linear gradient of water (0.1% TFA) and acetonitrile (0.1% TFA) with an initial water:acetonitrile ratio of 95:5 and a final ratio of 40:60. The products were then lyophilized and stored in sealed desiccated containers at −15 °C until use.

Acetylation of MP-11. MP-11 was purchased from Sigma (St. Louis, MO) and used without further purification. MP-11 was mixed with a 50-fold excess of acetic acid *N*-hydroxysuccinimide ester (AcOSu) in 50 mM tris-HCl buffer at pH 8.5 with a final concentration of about 1 mM, and the resulting mixture was stirred at room temperature for 4 h. The mixture was then passed through a 12 × 600 mm Bio-Gel P-2 (Bio-Rad) column to remove the excess reagents or incompletely acetylated MP-11. The crude product was further purified on a C18 column (25 × 250 mm) using HPLC eluted with 0.1% TFA and a gradient of 5−60% acetonitrile in the mobile phase. The product (MP-11 acetylated at both lysine and terminal amino groups) was recovered by lyophilization and stored at −15 °C until use.

Association Constant Determination. The association constant for the complexation between the RuProHis peptide and the heme of acMP-11 was determined by direct quantitation of the ratio of five- and six-coordinate heme components using a classical least-squares (CLS) method.[11] A calibration data set was collected using a tandem 5 mm path length divided cell. Thirty independent samples were synthesized by randomly changing the concentrations of acMP-11 and the acMP-

(7) (a) McLanahan, S. F.; Darlinger, R. F.; Holler, F. J.; Kincaid, J. R. *J. Am. Chem. Soc.* **1985**, *107*, 4853. (b) See, for example: *Biological Applications of Raman Spectroscopy*; Spiro, T., Ed.; Wiley: New York, 1988; Vol. III.

(8) (a) Aron, J.; Baldwin, D. A.; Marques, H. M.; Pratt, J. M.; Adams, P. A. *Inorg. Biochem.* **1986**, *27*, 227. (b) Santucci, R.; Picciau, A.; Campanella, L. *Biochim. Biophys. Acta* **1995**, *1250*, 183.

(9) Larsen, R. W.; Findsen, E. W.; Nalliah, R. E. *Inorg. Chim. Acta* **1995**, *234*, 101.

(10) Peek, B. M.; Ross, G. T.; Edwards, S. W.; Meyer, G. J.; Meyer, T. J.; Erickson, B. W. *Int. J. Pept. Protein Res.* **1991**, *38*, 114.

(11) Haaland, D. M.; Esterling, R. G. *Appl. Spectrosc.* **1980**, *34*, 539.

11/imidazole complex in each side of the tandem cell to average the possible concentration dependence of the chromophore and experimental error. The spectral data collected from these samples were used to generate a CLS calibration model. The spectra of the acMP-11/RuProHis sample were obtained by utilizing known concentrations of acMp-11 and RuProHis. Three samples with different concentrations and different RuPeptide:acMP-11 ratios were studied. The five-coordinate and six-coordinate compositions were then calculated using the calibration model.

Luminescence titrations were performed with anaerobic 10 mM ruthenium peptide solutions to which aliquots of a degassed 1 mM stock solution of acMP-11 were added using a gastight syringe.

Data Processing. Analysis of the time-resolved luminescence data was performed with an ENZFITER program in order to extract reasonable estimates of k_{ET} and K_a (see below). All data were fit using single-exponential or double-exponential functions. For the single-exponential fitting, the equation

$$I(t) = c + A_0 \exp(-k_0 t) \quad (1)$$

was used. A_0 and c represent the magnitude of the kinetic phase and the background, respectively, and k_0 is the intrinsic luminescence decay rate constant. The relative luminescence intensity, A, was corrected for reabsorption effects using an extinction coefficient of 874 M^{-1} cm^{-1} at the detection wavelength 670 nm. No inner-filter correction was applied since the sample was saturated by the pulsed excitation. Because the instrument response time is comparable to the ET rate, the complexed RuProHis can be assumed to be "dark" under the experimental conditions without introducing significant error into the estimation of the luminescent intensity of the slow phase (free RuProHis). The intensities thus estimated at different acMP-11 concentrations were then used to construct the Stern−Volmer plots using the pre-exponential term A of the free peptide as I_0.

Even though only a small portion of the overall decay kinetics can be detected in the current time-resolved studies, ET rates can still be estimated via double-exponential fitting using the k_0 value obtained in the Stern−Volmer analysis as a constant.

$$I(t) = c + A \exp[-(k_0 + k_{ET})t] + B \exp(-k_0 t) \quad (2)$$

In this expression, k_0 is the intrinsic luminescence decay rate of the free ruthenated peptide and k_{ET} is the rate constant for the quenching of excited state RuProHis via ET to the heme. Thus, $k_0 + k_{ET}$ is the net decay rate constant for the complexed species, and A and B represent the fractional magnitudes of the phases for the complexed and free ruthenated peptides, repectively. Bimolecular quenching was not explicitly included in the fitting procedure because, under our experimental conditions, it is far slower than either of the other two processes considered. It should also be noted that while electron transfer dominates the deactivation processes, the k_{ET} values obtained via the above procedures may reflect contributions from other pathways and thus represent upper limits to the actual electron transfer rates.

Molecular Modeling. All calculations were performed at Sandia National Laboratory using programs based on POLYGRAPH software (Molecular Simulation Inc.) but adapted with a force field specifically derived by Shelnutt and co-workers to yield accurate metalloporphyrin geometries.[12] The equilibrium Ru−N bond lengths of the $Ru(bpy)_3^{2+}$ complex were adjusted in order to maximize the correspondence between the computed energy-minimized structures and the crystal structures. The convergence condition was set to 0.001 kcal/(mol Å) rms force, and an approximation of the dielectric constant was used to shield the Coulombic interaction potentials and thus approximate solvent conditions. The initial structure of MP-11 was constructed from the appropriate fragment of the horse heart cytochrome *c* crystal structure acetylated at the two free amino groups. The initial structure of the peptide was constructed from a direct covalent linkage of the respective amino acids and the ruthenium group. The energies of both structures were then minimized separately. The initial structure of the RuProHis/acMP-11 complex was constructed by linking the heme iron and the imidazole nitrogen of the separately minimized acMP-11 and RuProHis structures. The energy of the complex was then minimized to obtain an equilibrium RuProHis/acMP-11 structure. In order to maximize the chances of finding a global minimum, simple dynamics at 300 K were run upon the initial structure prior to energy minimization. This was done several times for different durations (up to greater than 5 min), and the energy-minimized structure was always the same.

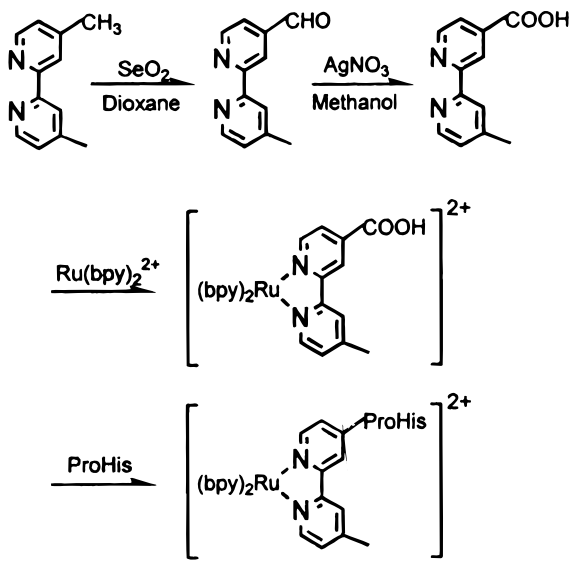

Figure 1. Synthesis scheme.

Results and Discussion

Synthesis and Equilibrium Characteristics. (a) Synthesis and Characterization of RuProHis. The $Ru(Pro)_nHis$ family of peptides is a convenient choice for a series of photoactive donors to the heme of MP-11. The photodynamic and spectroscopic properties of the derivatized $Ru(bpy)_3^{2+}$ are well-behaved and closely parallel those of free $Ru(bpy)_3^{2+}$. The structural rigidity the proline groups minimizes conformational flexibility of the peptide while the histidine imidazole provides for specific binding at the heme with reasonably high affinity (see below).

The procedure for peptide synthesis reported by Peek et al.[10] was modified for the synthesis of the ProHis dipeptide. This led to a product with CF_3COO^- as the counterion for the positively charged ruthenated peptides (instead of the PF_6^-), as confirmed by the laser desorption experiments, which show a strong peak at 113 with a negative m/z (data not shown). Two peaks were observed in the electrospray mass spectrum at m/z = 974 and 430, corresponding to $[M - TFA^-]^+$ (calculated to be 974) and $\{M - 2[TFA^-]\}^{2+}$ (calculated to be 430), respectively.

The ProHis dipeptide was linked to the $Ru(bpy)_3^{2+}$ moiety via the synthetic procedure shown in Figure 1. The pivotal step in the synthesis was the controlled transformation of a single methyl group of the dimethylbipyridyl ligand to form 4-methyl-4′-carboxybipyridine through SeO_2 oxidation. The corresponding ruthenium complex was then attached to the dipeptide through a standard solid phase synthesis procedure. Attachment of the RuProHis dipeptide to one of the bipyridine ligands causes small perturbations in some spectroscopic properties of the complex without inducing large structural changes. Absorption spectra show that the MLCT band maximum moves to 458 nm compared to 456 nm for $Ru(bpy)_3^{2+}$ (Figure 2A). Also, the emission maximum shifts from 613 nm for $Ru(bpy)_3^{2+}$ to 642 nm for RuProHis (Figure 2A). The ground state resonance Raman spectra (data not shown) are quite similar to those of $Ru(bpy)_3^{2+}$ except for the presence of two extra bands at 1541 and 1619 cm^{-1}.[7a] These are attributed to modes arising from the derivatized 4-methyl-4′-carboxybipyridine ligand.

(12) (a) Jentzen, W.; Simpson, M. C.; Hobbs, J. D.; Song, X.; Shelnutt, J. A. *J. Am. Chem. Soc.* **1995**, *117*, 11085. (b) Sparks, L. D.; Medforth, C. J.; Park M.-S; Ondrias, M. R.; Shelnutt, J. A. *J. Am. Chem. Soc.* **1993**, *115*, 581.

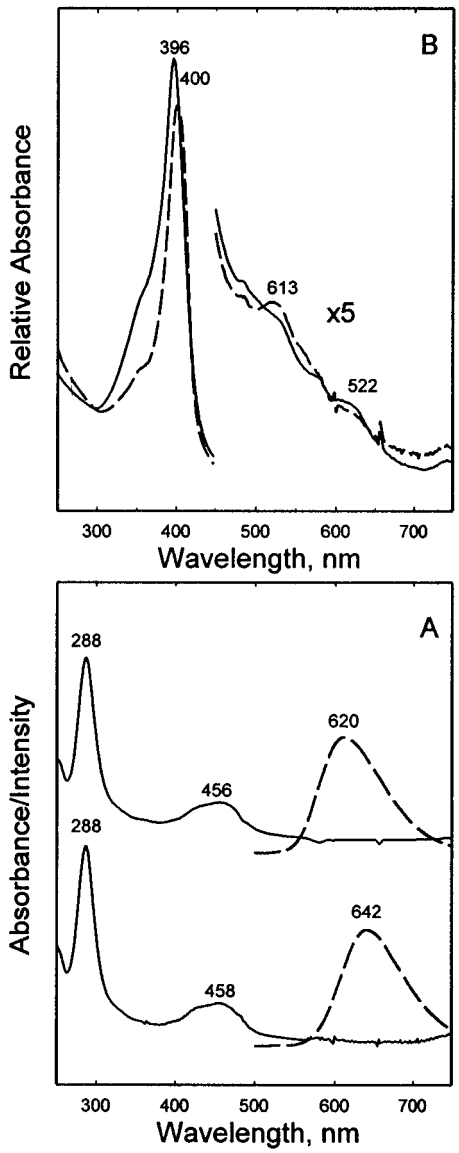

Figure 2. Optical absorption and luminescence properties of the RuProHis peptide. Panel A: UV−vis absorption (solid lines) and luminescence spectra (dashed lines) of $Ru(bpy)_3Cl_2$ (upper traces) and $Ru(bpy)_3$ProHis (lower traces). Spectra were obtained from 10 μM samples in 100 mM phosphate buffer at pH 7.0. The luminescence spectra were measured with 450 nm excitation at a scan rate of 60 nm/s and 2 nm resolution. Panel B: UV−vis absorption spectra of acMP-11 (solid line) and free MP-11 (dashed line). Samples were 1 mM in 100 mM phosphate buffer at pH 7.0.

(b) Acetylation of MP-11. One of the major limitations of microperoxidases as heme protein model systems is their tendency to aggregate in aqueous solutions.[13,14] The mechanism of the aggregation is generally believed to be a combination of hydrophobic interactions and intermolecular coordination between the α-amino group in the N-terminus valine or the ϵ-amino group on the lysine and the five-coordinate heme. Computer modeling results (see below) clearly show that the sixth ligation position of the MP-11 heme is quite open and exposed to solvent and thus are quite consistent with this scenario. In this study, a variety of strategies were employed to eliminate MP-11 aggregation and produce a homogeneous sample of ET model complexes. The use of more hydrophobic solvents (i.e., alcohols) significantly reduces aggregation but produces a less physiologically relevant environment.[8a] Similarly, detergents like CTAB,[15] at concentrations greater than their critical micellar concentrations, can disperse MP-11 and produce a homogeneous population of heme species. Unfortunately, the putative incorporation of MP-11 into micelles hinders the binding of exogenous ligands, particularly the ruthenated peptides.

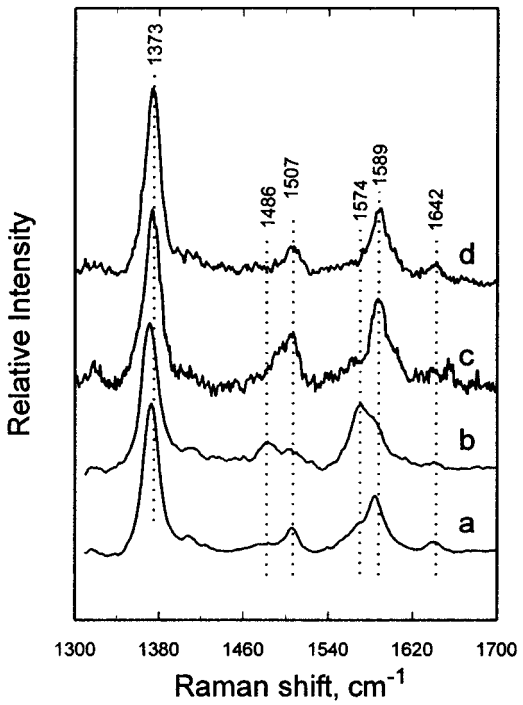

Figure 3. Resonance Raman spectra of different microperoxidase species: (a) MP-11; (b) acMP-11; (c) 1:1.5 mixture of acMP-11 and RuProHis; (d) acMP-11 in 100 mM imidazole. All spectra were taken in 5 mM phosphate buffer at pH 7.0 using 406 nm excitation (∼0.3 mJ/pulse). Samples were ∼100 μM for all MP-11.

The most effective means of suppressing aggregation proved to be the direct acetylation of the terminal amino groups of MP-11 via a modification of the method of Wang et al.[14] In the present study, a modified procedure using AcOSU, rather than an excess of acetic anhydride, was employed to acetylate MP-11. The acetylated MP-11 (acMP-11) was characterized spectroscopically. While absorption spectra (Figure 2B) of aggregated MP-11 display characteristics of low-spin hemes, acMp-11 spectra show a predominance of high-spin species. This is most evident in the position of the Soret band for ferric acMP-11 (396 nm vs 406 nm) and concomitant changes in the 500−700 nm region, including the presence of a new band at 630 nm and the marked reduction of the characteristic 530 nm Q band of low-spin hemes.

Resonance Raman spectroscopy (RRS) has been applied to the characterization of heme proteins for several decades. Heme vibrational spectra are quite sensitive to the electronic and structural nuances of the porphyrin marcrocycle. In particular, the high-frequency heme modes display a systematic sensitivity to heme ligation and spin state.[7b] The RRS spectra of MP-11 species show convincingly that a low- to high-spin conversion of the heme occurs upon acetylation (Figure 3). The spin-state-sensitive bands ν_2, ν_3, and ν_{10} all show intensity shifts commensurate with a large increase in high-spin heme population in the acMP-11 sample relative to aggregated (low-spin) MP-11. The behaviors of ν_3 (∼1485 cm^{-1} for high spin, ∼1507 cm^{-1} for low spin) and ν_2 (∼1574 cm^{-1} for high spin, ∼1588 cm^{-1} for low spin) in the RR spectra of MP-11 are also particularly sensitive to the heme ligation state.[14,7b] Figure 3

(13) Urrry, D. W. *J. Am. Chem. Soc.* **1967**, *89*, 4190.
(14) Wang, J. S.; Van Wart, H. E. *J. Phys. Chem.* **1989**, *93*, 7925.
(15) Othman, S.; LeLirzin, H.; Desbois, A. *Biochemistry* **1993**, *32*, 9781.

clearly shows a large increase in the lower energy components of these bands at ~1486 cm^{-1} (ν_3), ~1574 cm^{-1} (ν_2), and ~1620 cm^{-1} (ν_{10}), indicative of a population shift toward five-coordinate high-spin hemes in the acMP-11 sample. The higher energy shoulders for both ν_2 and ν_3 in the acMP-11 spectrum indicate the existence of a minor heme species having different spin/ligation states. These could include six-coordinate low-spin ($S = {}^1/_2$) species due to coordination of OH^- in solution and/or an $S = {}^3/_2$ five-coordinate species. The first possibility is doubtful in view of the insensitivity of the RR spectra over a pH range of 4.7−8.7 (data not shown). In proteins, the octahedral field of six-coordinate Fe in heme may be distorted because of changes in the axial ligation.[16] This distortion of the axial ligand may lead to the lowering of the symmetry from octahedral to tetragonal, thus breaking the degeneracy of the e_g (d_{z^2}, $d_{x^2-y^2}$) orbitals and allowing the intermediate-spin state to occur. In any event, it appears that, under ambient solution conditions, acMP-11 exists as a thermal equilibrium dominated by the five-coordinate high-spin heme species.

Similar behavior was previously observed for acetylated heme−octapeptide species by Van Wart and co-workers.[14] They found that the room temperature resonance Raman spectra of acMP-8 exhibit two sets of porphyrin skeletal stretching frequencies in the high-frequency region and concluded that the species responsible for the higher frequency set of bands is an intermediate-spin (either pure intermediate ($S = {}^3/_2$) or quantum-admixed intermediate ($S = {}^3/_2$)−high ($S = {}^5/_2$) spin) form of acMP-8. They further speculated that the $S = {}^3/_2$ state resulted from the weak bonding interaction between histidine-18 and the heme. The data obtained in this study are quite consistent with the observations of Van Wart et al. Not surprisingly, once all of the free amino groups are acetylated, the slightly longer peptide does not cause additional perturbation of the heme and the resonance Raman behavior of acMP-11 is quite simlar to that of acMP-8.

RuProHis/acMP-11 Complexation. The application of simple titration methodologies to determine the association constant for RuProHis and acMP-11 was complicated by the overlapping $Ru(bpy)_3^{2+}$ and heme absorption bands and by the limited availability of RuProHis. Thus, the association constant of RuProHis/acMP-11 was determined by direct quantitation of the five- and six-coordinate components in the equilibria of known analytical concentrations via classical least-squares protocols described in detail in ref 11. The association constant for the simple equilibrium complexation of acMP-11 and RuProHis can be readily expressed as

$$K_a = \frac{[MP/RuP]}{\{[MP]_0 - [MP/RuP]\}\{[RuP]_0 - [MP/RuP]\}} \quad (3)$$

where $[MP]_0$ and $[RuP]_0$ refer to the initial concentratrations of acMP-11 and RuProHis, respectively, and [MP/RuP] is the concentration of the complex. A representative calibration spectrum used to obtain the fractional populations of complexed and free acMp-11 is shown in Figure 4. The association constant was calculated to be $(1.4 \pm 0.5) \times 10^4$ M^{-1}. The marked increase in K_a for the complexation of RuProHis/acMP-11 compared to that of histidine (4000 M^{-1}) (as determined by direct titration methods; data not shown) can be attributed largely to increased hydrophobic interactions between acMP-11 and RuProHis. This scenario is supported by the molecular modeling results (see below).

Resonance Raman spectra also demonstrate the formation of a low-spin heme adduct in the presence of both imidazole and RuProHis. Figure 2 clearly shows the quantitative conversion of acMP-11 to a low-spin species in the presence of excess imidazole. Here again, the behavior of ν_3 and ν_2 demonstrates this effect. The isolated, narrow bands for both ν_2 (~1640 cm^{-1}) and ν_3 (~1507 cm^{-1}) are diagnostic for a homogeneous population of low-spin, six-coordinate hemes. The RR spectrum of the 1:1.5 acMP-11:RuProHis mixture shows nearly complete conversion from five-coordinate to six-coordinate species upon ligation of the short peptide, indicated by the disappearance of the high-spin ν_2 at 1574 cm^{-1}. The ν_3 region is complicated by the contribution of the 1490 cm^{-1} band arising from the $Ru(bpy)_3^{2+}$ group.[7a] A higher degree of six-coordinate complexation can, of course, be achieved by using higher peptide concentration, but the RR spectra of the ground state acMP-11/RuProHis samples will be too complicated at high peptide concentration because of the presence of the bipyridine bands in the heme ν_2 and ν_3 regions.

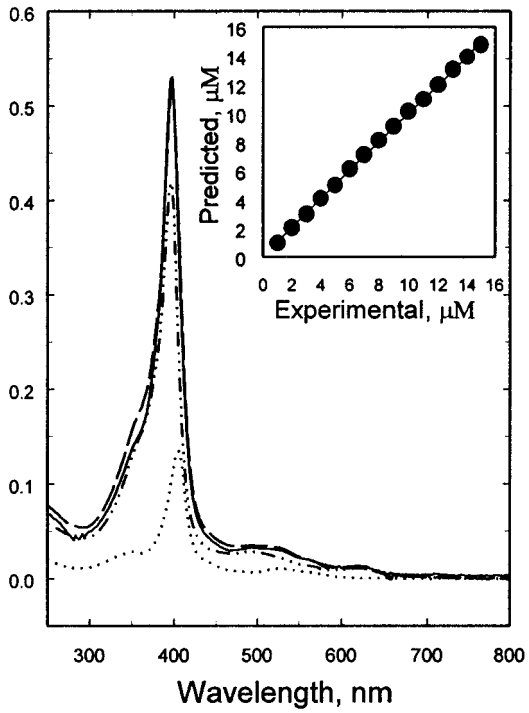

Figure 4. CLS quantitation of the five-coordinate and six-coordinate components in the mixture of RuProHis/acMP-11. The main figure shows the results of the deconvolution of the spectrum of a mixture of 40.2 μM RuProHis and 18.3 μM acMP-11 in 100 mM phosphate, pH 7.0: solid line, raw spectrum; dashed line, calculated spectrum; dot-dashed line, spectrum of the five-coordinate component; dotted line, spectrum of the six-coordinate component. The inset depicts the calibration curve obtained from the imidazole/acMP-11 titration for the actual vs calculated fractions of the five-coordinate (i.e., free acMP-11) component. Measurements were performed at three different RuProHis:acMP-11 ratios and/or concentrations and yielded an average K_a of $(1.4 \pm 0.5) \times 10^4$ M^{-1} according to eq 3.

(d) Modeling of the RuProHis/acMP-11 Structure. The energy minimized molecular structure of RuProHis complexed with acMP-11 is shown in Figure 5. A variety of energy minimization protocols were employed, including using different starting points for the structural minimization and different dielectric constants. In all cases, energy minimization of the acMP-11/RuProHis complexes revealed a strong enthalpic driving force for complexation. The final calculations were performed using the dielectric constant of water since all of the spectroscopic studies were performed in aqueous solution. The energetic parameters thus derived are listed in Table 1.

The data in Figures 3 and 4 unequivocally show that RuProHis forms a relatively tight complex with microperoxidase

(16) Moore, G. R.; Pettigrew, G. W. *Cytochrome c*; Springer-Verlag: New York, 1990.

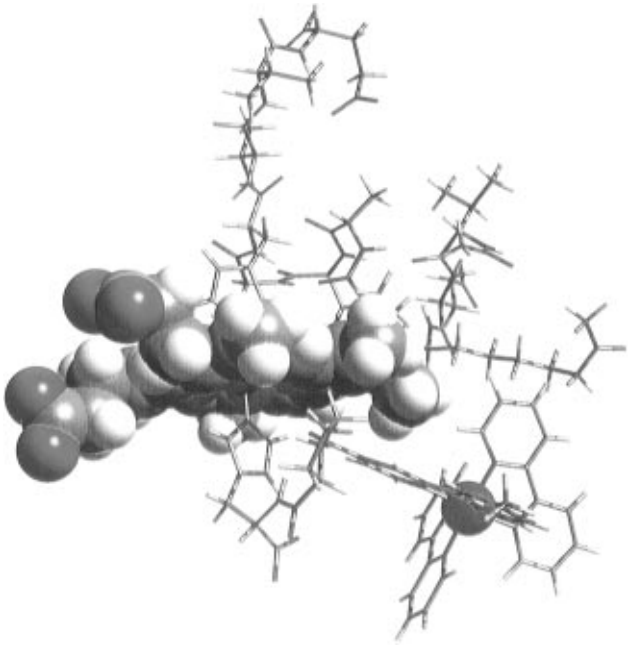

Figure 5. Computer-modeled structure of the complex between RuProHis and acMP-11. See text for details of modeling protocols.

Table 1. Energetic and Structural Parameters of Computer-Simulated Microperoxidase and RuProHis Structures[a]

	acMP-11	RuProHis	complex	ΔE[b]
total energy	228.25	141.98	351.19	−19.04
bonds	20.84	10.20	33.19	2.15
angles	142.4	42.02	186.63	2.21
torsion	33.09	13.80	48.41	1.52
inversion	1.86	0.05	2.06	0.15
van der Waals	80.68	80.37	137.21	−23.84
electrostatics	−1.18	0.12	−1.68	−0.62
H-bonds	−49.43	−4.57	−54.64	−0.64
R_{Ru-Fe}, Å, through-space			12.08	
R_{Ru-Fe}, Å, through-bond			22.38	
$R_{edge-edge}$,[c] Å, through-space			8.02	

[a] All structures are minimized at a dielectric constant of 79*r*; all energies are in kcal/mol. [b] $\Delta E = E_{total}$[RuProHis/MP-11] − (E_{total}[RuProHis] − E_{total}[acMP-11]). [c] $R_{edge-edge}$ is the closest contact distance between the heme and the $Ru(bpy)_3^{2+}$ group.

compared to similar nitrogenous ligands, such as imidazole or histidine. The importance of hydrophobic (van der Waals) interactions in the equilibrium ligation behavior of acMP-11 is also supported by observations of the aggregation behavior of microperoxidases. For instance, the large hydrophobic contribution to the aggregation is evidenced by the fact that the dimerization constant, K_D, decreases upon increasing the solvent hydrophobicity, from 117 000 M^{-1} in H_2O to 2160 M^{-1} in 50% (v/v) methanol/H_2O.[8a] Large hydrophobic contributions have also been observed in other model systems. In particular, the complexation between the heme-containing N-terminal fragment (residues 1−38) and a synthetic peptide corresponding to the C-terminus helix of cytochrome *c* (residues 87−104) exhibits a large association constant (1×10^6 M^{-1}), even though no coordinative ligand is involved in the association process.[17] A histidine-containing peptide (13 amino acids) has been reported to form a tight complex with MP-11 (4.8×10^4 M^{-1}).[8b] It is also apparent that axial coordination of the heme plays an important role in the aggregation process since the aggregation is greatly reduced by acetylation of the terminal amino group, which is believed to be responsible for intermolecular ligation

(17) Wu, L. C.; Laub, P. B.; Elove, G. A.; Carey, J. C.; Roder, H. *Biochemistry* **1992**, *32*, 10271.

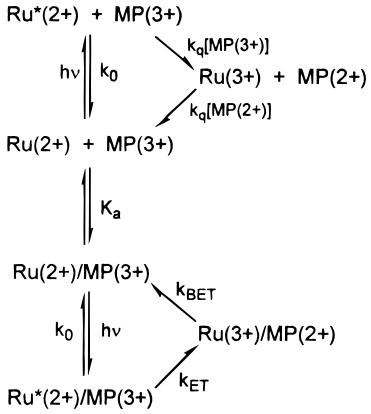

Figure 6. Photochemical cycle of possible electron transfer processes in the RuProHis/acMP-11 system. k_{ET} is the electron transfer rate constant, k_{BET} is the back electron transfer rate constant, k_q is the intrinsic decay rate constant, and K_a is the ground state equlibrium constant.

to the five-coordinate heme. Together, these observations suggest that a combination of imidazole coordination and hydrophobic interactions between the bpy group and the heme is responsible for the large association constants of the acMp-11/RuProHis systems.

Computer modeling further illustrates the multiple origins of the significant energy drop that must accompany complexation (Table 1). A total energy drop, ΔE, of ∼19 kcal/mol, is engendered by complexation. The calculated stabilization energy is considerably larger in the ruthenated peptide complexes than in the complex with free histidine (2.9 kcal/mol; data not shown). Indeed, the majority of the stabilization energy comes from van der Waals interactions. (−23.8 kcal/mol). In contrast, electrostatic interactions apparently play lesser roles in the complexation process most likely because of the high dielectric constant of the aqueous solution.

Despite the tight association of acMP-11 and RuProHis, the electron transfer distances within the complex remain relatively large. The energy-minimized conformation exhibits a dramatic difference in the through-bond (22.4 Å) and through-space distances (12.1 Å) between Ru and the Fe center (see Table 1). These are comparable to the through-space distances in horse heart cytochrome *c* ruthenated at lysine-72.[5c,d]

Electron Transfer Dynamics. The $Ru(Pro)_n$His/acMP-11 systems provide a versatile set of models for the study of photoinitiated electron transfer in a biologically relevant setting. Absorption of a photon to create a $Ru(bpy)_3^{2+}$* species can initiate both bi- and unimolecular photodynamics as shown in Figure 6. Fortunately, equilibrium conditions can be manipulated in order to restrict the majority of photoinitiated activity to intracomplex dynamics. In addition, the spectroscopic properties of both the donor ($Ru(bpy)_3^{2+}$*) and acceptor (ferric heme) can be exploited in separate time-resolved experiments (luminescence and resonance Raman, respectively) to extract both the kinetics and structural dynamics as associated with photoinduced electron transfer. The initial spectroscopic data obtained in this study indicate that rapid, efficient ET can be photoinitiated in the acMP-11/RuProHis complexes.

(a) Transient Resonance Raman (TRR) Experiments. Heme resonance Raman spectra are very sensitive to the iron oxidation state. For instance, the equilibrium ferric and ferrous acMP-11/imidazole complexes exhibit dramatic spectral changes upon heme reduction. The largest of these is the shift of the oxidation state marker ν_4 from 1373 cm^{-1} for ferric heme to 1360 cm^{-1} for ferrous heme. Thus the TRR spectra can be used to qualitatively monitor the kinetics of photoinitiated ET in the RuProHis/acMP-11 systems.

The protocol employed in this study was previously used

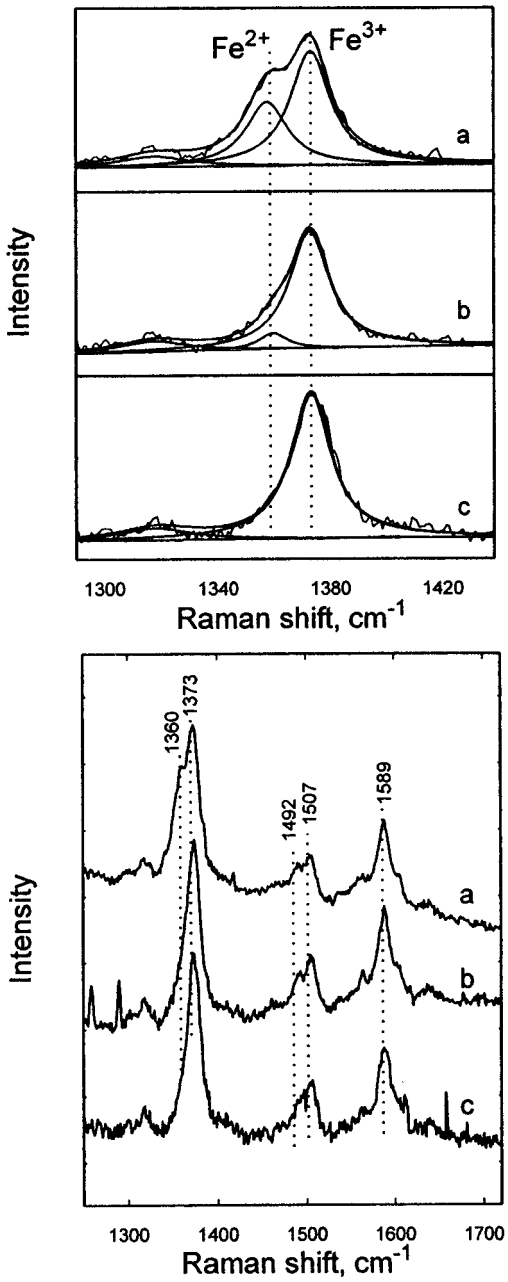

Figure 7. Transient Raman spectra of a 1:1.5 mixture of RuProHis and acMP-11: (a) high power (0.75 mJ/pulse); (b) medium power (0.18 mJ/pulse); and (c) low power (0.075 mJ/pulse). The lower panel displays the entire high-frequency region. Spectra were taken with 416 nm excitation at 10 Hz. Laser power was controlled using neutral density filters. The sample contained 100 μM acMP-11 and 100 mM phosphate buffer at pH 7.0. The upper panel depicts a further analysis of the behavior of ν_4. Spectra were fit with Lorentzian line shapes to display the relative contributions of ferrous ($\sim$1360 cm^{-1}) and ferric ($\sim$1370 cm^{-1}) heme scattering using previously described methods.[18]

to investigate the electron transfer dynamics of ruthenated cytochrome *c* using pulses from a single laser source to both initiate ET (by exciting the Ru(bpy)$_3^{2+}$ donor) and generate a spectrum of the reduced acceptor (via resonant scattering from the heme).[18] Thus the TRR spectra reflect the net dynamics of the system within the 10 ns laser pulses. In this case, the magnitude of ferrous heme vibrational bands in the TRR spectrum depends upon both the photon fluxes of the excitation pulses and the kinetics of the ET process. TRR spectra of a

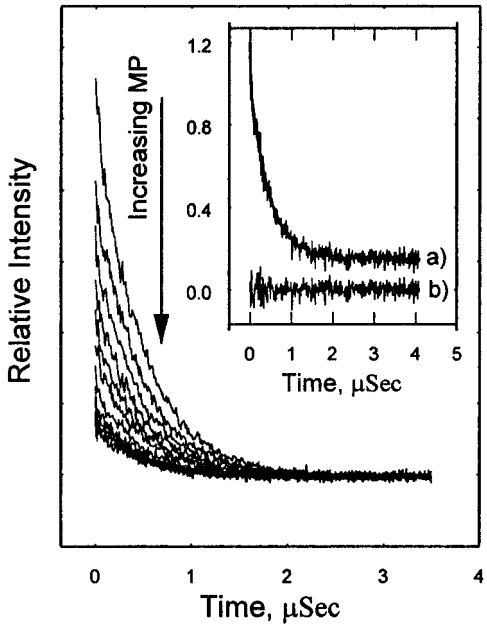

Figure 8. Transient luminescence titration curves of RuProHis (10 μM) at acMP-11 concentrations from 0.0 to 65 μM in 5 μM increments. Samples were prepared in 5 mM phosphate buffer at pH 7.0. Spectra were obtained using 532 nm excitation and detected at 670 nm. The inset shows (a) the double-exponential fit for the data obtained from 50 μM acMP-11 in the presence of 50 μM RuProHis, giving $A = 2.3 \times 10^{-4}$, $B = 9.0 \times 10^{-4}$, and $k_{ET} = 4.2 \times 10^7$ s^{-1}, and (b) the residuals for the fit (see text for details).

1:1.5 mixture of acMP-11 and the RuProHis complex are shown in Figure 7. At low laser flux, ν_4 occurs as a single narrow band at 1371 cm^{-1} indicative of ferric heme, but at elevated laser flux, a power-dependent growth of a transient band at 1360 cm^{-1} indicates a significant photoreduction of the heme within the 10 ns width of the excitation pulse. The power dependence of this rapid photoreduction as reflected by the behavior of ν_4 clearly shows that the ET process is largely reversible and is intramolecular.

(b) Luminescence Experiments. The strong quenching of RuProHis luminescence by acMP-11 provides irrefutable evidence for the existence of alternative deactivation pathways for photoexcited Ru(bpy)$_3^{2+}$* within the complex. The observation of reduced heme bands in the nanosecond TRR spectra conclusively confirm that rapid electron transfer occurs from Ru(bpy)$_3^{2+}$ to the ferric heme. Time-resolved luminescence measurements were used to quantify the kinetics of this process. The results of the time-resolved luminescence titrations are shown in Figures 8 and 9. Because the data contain multiple kinetic phases and the exact contribution from each phase is not known, single-exponential fitting cannot be interpreted in an unambiguous and quantitative manner. However, several qualitative points are still evident concerning the nature of the ET process. First, the I_0/I Stern−Volmer plot of RuProHis quenching an upward curvature compared to the t_0/t plot (Figure 9). This is characteristic behavior for systems where static quenching of luminescence exists.[19] Second, the possibility of significant electrostatic interaction between the positively charged Ru(bpy)$_3^{2+}$ and the negatively charged acMP-11 can be ruled out by the results of a control experiment utilizing the free Ru(bpy)$_3^{2+}$ and acMP-11. In the case of free Ru(bpy)$_3^{2+}$, the congruence of the intensity plot and the lifetime plot indicates no significant electrostatic complexation. Also, when the titration was performed in the presence of imidazole (data not shown), the magnitude of the upward curvature of the

(18) (a) Simpson, M. C.; Millett, F.; Fan, B.; Ondrias, M. R. *J. Am. Chem. Soc.* **1995**, *117*, 3296. (b) Simpson, M. C.; Millett, F.; Pan, L. P.; Larsen, R. W.; Hobbs, J. D.; Fan, B.; Ondrias, M. R. *Biochemistry* **1996**, *35*, 10019.

(19) White, H. S.; Becker, W. G.; Bar, A. J. *J. Phys. Chem.* **1984**, *88*, 1840.

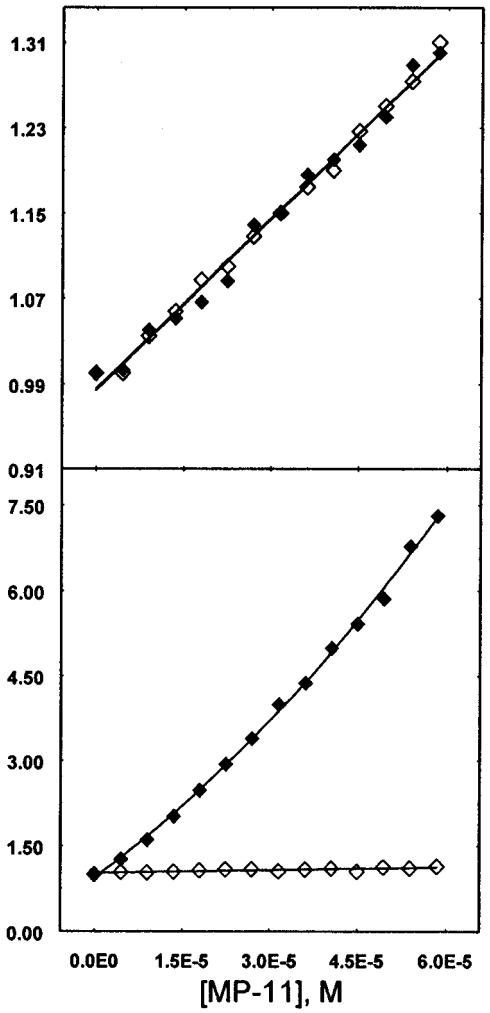

Figure 9. Stern−Volmer plots of the luminescence titration for RuProHis (lower panel) and $Ru(bpy)_3^{2+}$ (upper panel). In both panels, open diamonds refer to lifetime plots, τ_0/τ, and solid diamonds refer to intensity plots, I_0/I. Experimental conditions are exactly the same as described in the caption of Figure 7. See text for details.

intensity plot was greatly decreased. The results of these control experiments prove that the static quenching of the photoexcited $Ru(bpy)_3^{2+}$ analog occurs through coordination of RuProHis to the heme iron.

Multiple decay pathways coexist in the photoexcited mixture of acMP-11 and RuProHis. These include the intrinsic decay of free $Ru(bpy)_3^{2+}$*, intramolecular ET within RuProHis/acMP-11 complexes, and collisional ET quenching of free RuProHis by free acMP-11. Under our experimental conditions (<100 μM acMP-11), the contribution from the bimolecular process is much smaller than both the intrinsic decay and the intramolecular ET and can be neglected. Thus luminescence decay can be fitted with a biexponential decay function (eq 2) to extract the ET rate constant (k_{ET}) given that k_0 is known from the measurement of the intrinsic lifetime of RuProHis. At the extremes of acMP-11 concentration (e.g., below 20 μM or above 60 μM), double-exponential fitting of the time-resolved luminescence decay data is inaccurate because of either the small fraction of the intramolecular process or poor S/N ratio. Thus, analysis was performed with data obtained from 50 mM acMP-11, which gives a balance of five- and six-coordinate populations and reasonable S/N. Fitting results can be used to estimate both the electron transfer rate and the binding constant according to a modified procedure developed by Harriman and co-workers,[20] where the fractional magnitudes of the two components are used for the estimation of the binding constant:

$$K_a = \frac{P_0A(A+B)}{[(A+B)M_0 - AP_0]BP_0} \quad (4)$$

Here A and B are the fractional magnitudes of the two phases (as determined by eq 2) and M_0 and P_0 are the analytical concentrations of MP-11 and RuProHis, respectively. The value of the association constant calculated via this method ($\sim 3 \times 10^4$ M^{-1}) is reasonably consistent with the results of CLS analysis (Figure 3). An ET rate constant of 4.2×10^7 s^{-1} was obtained. It should be noted that this rate constant represents an upper limit since it potentially contains contributions from other deactivation processes like energy transfer (see the following article for a discussion of energy transfer vs electron transfer in ruthenium/MP systems). Nonetheless, it is quite consistent with the appearance of a measurable amount of ferrous heme in the 10 ns transient resonance Raman spectra of the acMP-11/RuProHis complex (Figure 6) and other studies of similar systems.[5c]

Conclusions

The results of this study demonstrate that robust, well-characterized model electron transfer systems can be rationally designed and synthesized using heme protein active site analogs and novel ruthenated peptide ligands. Both spectroscopic and molecular modeling methods were employed to determine the equilibrium characteristics of isolated acMP-11 and its coordination behavior with RuProHis. The data clearly indicate that complexation of RuProHis occurs at the open sixth ligand site of the heme iron in MP-11 via the His moiety. Transient resonance Raman and time-resolved luminescence measurements further indicate that rapid, reversible electron transfer ($k_{ET} > 10^7$ s^{-1}) from the $Ru(bpy)_3^{2+}$* analog to the ferric heme can be photoinitiated with visible light.

The acMP-11/RuProHis system is prototypic of a large class of Ru−peptide−His species where the peptide spacer can be tailored via solid phase peptide synthesis to probe different aspects of protein mediated ET. For instance, rigid polyproline spacers could be used to determine distance dependence of ET rates while other amino acid combinations could be employed to test effects of the general peptide environment (hydrophobicity etc) on the regulation of ET processes. These initial studies provide the basis for the systematic investigation of the photoinitiated electron transfer dynamics of a variety of related model systems (see following article) currently underway in our laboratories.

Acknowledgment. This work was supported by the NIH (Grant GM33330 to M.R.O.), the Petroleum Research Fund, administered by the American Chemical Society (Grant PRF2851064 to R.W.L.), DOE (Contract DE-ac04-94al85000 to J.A.S.), and the Department of Energy Distinguished Postdoctoral Research Program (M.C.S.). We thank A. Pastuszyn and the Cancer Center Protein Core Facility of the University of New Mexico for invaluable assistance.

IC9700415

(20) Sessler, J. L.; Capuano, V. L.; Kubo, Y.; Johnson, M. R.; Magda, D. J.; Harriman, A. H. In *Photoprocesses in Transition Metal Complexes, Biosystems and Other Molecules*; Kochanski, E., Ed.; Kluwer Academic Publishers: Boston, MA, 1991.